

Mechanics-guided embryonic patterning of neuroectoderm tissue from human pluripotent stem cells

Xufeng Xue^{1,9}, Yubing Sun^{1,2,9*}, Agnes M. Resto-Irizarry¹, Ye Yuan³, Koh Meng Aw Yong¹, Yi Zheng¹, Shinuo Weng ¹, Yue Shao ¹, Yimin Chai⁴, Lorenz Studer^{5,6} and Jianping Fu ^{1,7,8*}

Classic embryological studies have successfully applied genetics and cell biology principles to understand embryonic development. However, it remains unresolved how mechanics, as an integral driver of development, is involved in controlling tissue-scale cell fate patterning. Here we report a micropatterned human pluripotent stem (hPS)-cell-based neuroectoderm developmental model, in which pre-patterned geometrical confinement induces emergent patterning of neuroepithelial and neural plate border cells, mimicking neuroectoderm regionalization during early neurulation in vivo. In this hPS-cell-based neuroectoderm patterning model, two tissue-scale morphogenetic signals—cell shape and cytoskeletal contractile force—instruct neuroepithelial/neural plate border patterning via BMP-SMAD signalling. We further show that ectopic mechanical activation and exogenous BMP signalling modulation are sufficient to perturb neuroepithelial/neural plate border patterning. This study provides a useful microengineered, hPS-cell-based model with which to understand the biomechanical principles that guide neuroectoderm patterning and hence to study neural development and disease.

ne of the enduring mysteries of biology is tissue morphogenesis and patterning, where embryonic cells act in a coordinated fashion to shape the body plan of multicellular animals¹⁻⁵. As a highly conserved developmental event crucial for the nervous system formation, neural induction, for example, leads to differentiation of the ectoderm into a patterned tissue, containing the neuroectoderm (neural plate, or NP) and the epidermal ectoderm separated by the neural plate border (NPB) (Fig. 1a)^{6,7}. Classic embryological studies of neural induction have unravelled the importance of graded developmental signalling mediated by diffusible signals such as bone morphogenetic proteins (BMPs) (Fig. 1a)8-10. However, neural induction, like any tissue-scale morphogenetic event, occurs within the milieu of biophysical determinants, including changes in shape, number, position and force of cells^{7,11}. Yet it remains undetermined how these tissue-scale morphogenetic changes work in concert with classic developmental signaling events mediated by diffusible signals for proper cell fate patterning during neural induction.

hPS cells, which reside in a developmental state similar to the pluripotent epiblast^{12,13}, have been successfully used for the development of self-organized models of human embryonic development¹⁴⁻²¹. To date, however, no neural induction models exist that leverage hPS cells and their innate self-organizing properties to study neuroectoderm patterning. Here, we sought to develop micropatterned hPS-cell colonies on two-dimensional substrates to model neural induction. Microcontact printing was utilized to generate vitronectin-coated, circular adhesive islands with a diameter of 400 µm on flat poly-dimethylsiloxane (PDMS) surfaces coated

on glass coverslips (Fig. 1a and Supplementary Fig. 1). H1 human embryonic stem (hES) cells were plated as single cells at 20,000 cells cm $^{-2}$ on adhesive islands to establish micropatterned colonies with a defined circular shape and size. A differentiation medium supplemented with the dual SMAD inhibitors, SB 431542 (SB, TGF- β inhibitor; 10 μ M) and LDN 193189 (LDN, BMP4 inhibitor; 500 nM), was applied for neural induction 22 (Supplementary Fig. 1; see Methods). The β -catenin stabilizer CHIR 99021 (CHIR, 3 μ M), a WNT activator, was also supplemented in culture (Supplementary Fig. 1). CHIR promotes NPB cell specification under the neural induction condition established by the dual SMAD inhibitors 23,24 .

Although cells distributed uniformly on adhesive islands 24h after initial cell plating, neural induction resulted in differentiating cells gradually accumulating in the colony central area, leading to a significantly greater cell density at the colony centre than at the periphery (Fig. 1b and Supplementary Fig. 1). Cell density was further analysed using DAPI fluorescence intensity. The full width at half maximum (FWHM) for spatial distributions of DAPI intensity decreased continuously from 336 µm at day 1 to 240 µm at day 9 (Supplementary Fig. 1). Confocal images further showed that micropatterned colonies at day 7 remained as a monolayer. Strikingly, quantitation of colony thickness and nucleus shape revealed that at this point, cells exhibited a gradual change of cell shape from a columnar phenotype with columnar nuclei at the colony centre to a cuboidal morphology with rounded nuclei at the colony periphery (Supplementary Fig. 1), consistent with characteristic neuroectoderm thickening during neural induction in vivo^{6,11}. Importantly, Pax6+ neuroepithelial (NE) cells, the neural progenitor

¹Department of Mechanical Engineering, University of Michigan, Ann Arbor, MI, USA. ²Department of Mechanical and Industrial Engineering, University of Massachusetts, Amherst, MA, USA. ³School of the Gifted Young, University of Science and Technology of China, Hefei, China. ⁴Department of Orthopedic Surgery, Shanghai Jiao Tong University Affiliated Sixth People's Hospital, Shanghai, China. ⁵Developmental Biology Program, Memorial Sloan-Kettering Institute, New York, NY, USA. ⁶Center of Stem Cell Biology, Memorial Sloan-Kettering Institute, New York, NY, USA. ⁷Department of Biomedical Engineering, University of Michigan, Ann Arbor, MI, USA. ⁸Department of Cell and Developmental Biology, University of Michigan Medical School, Ann Arbor, MI, USA. ⁹These authors contributed equally: Xufeng Xue, Yubing Sun *e-mail: ybsun@umass.edu; jpfu@umich.edu

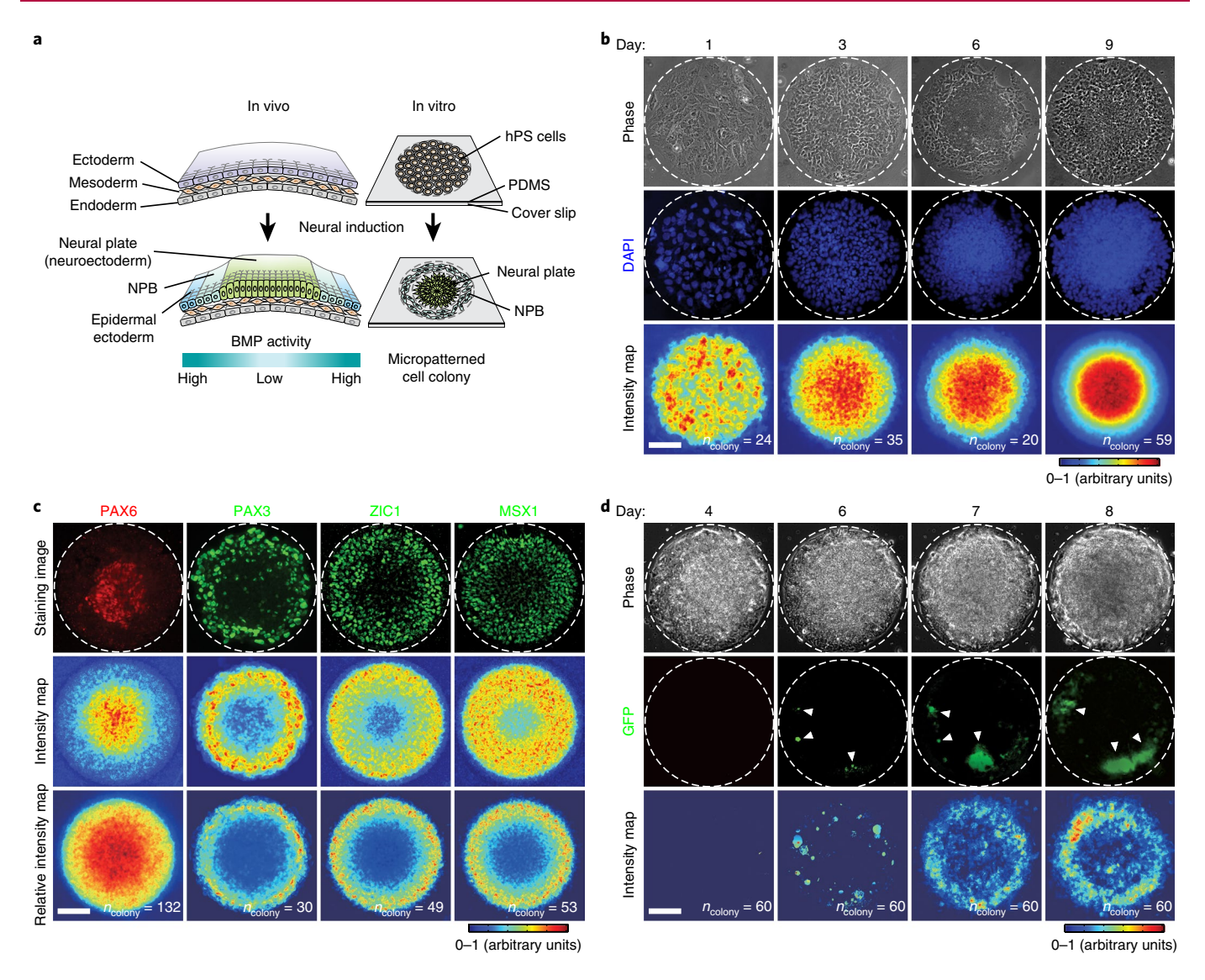


Fig. 1 Self-organized neuroectoderm patterning in circular hPS cell colonies. **a**, Schematic of neural induction in vivo and in vitro. During neural induction in vivo, embryonic cells in the ectoderm form the neural plate (neuroectoderm). Embryonic cells at the neural plate border (NPB) separate the neuroectoderm from the epidermal ectoderm. Neural induction of circular hPS cell colonies leads to autonomously patterned neuroectoderm tissues, with neural plate cells in the colony central region and NPB cells at the colony periphery. **b**, Representative phase contrast and fluorescence images showing cell morphology and nuclei (stained by DAPI), respectively, on different days. White dashed lines mark the colony periphery. Experiments were repeated three times with similar results. Bottom average intensity maps show spatial distributions of DAPI intensity. The number of colonies analysed was pooled from n = 3 independent experiments. Data plotted are mean values. **c**, Representative immunofluorescence micrographs and average intensity maps showing colonies at day 9 stained for neuroectoderm marker Pax6 and NPB markers Pax3, Zic1 and Msx1. White dashed lines mark the colony periphery. Experiments were repeated three times with similar results. Relative intensity maps were normalized to DAPI signals. The number of colonies analysed was pooled from n = 3 independent experiments. Data plotted are mean values. **d**, Representative phase contrast and fluorescence images and average intensity maps from live cell assays using Sox10-EGFP hES cells. White dashed lines mark the colony periphery. White arrowheads mark GFP+ cells at the colony border. Experiments were repeated three times with similar results. The number of colonies analysed was pooled from n = 3 independent experiments. Scale bars in **b-d**, 100 μm.

in the NP, were found preferentially localized at the colony central region on day 9, whereas Pax3+, Zic1+ and Msx1+ NPB cells were concentrated at the colony periphery, forming a concentric ring-shaped tissue sheet consistent with neuroectoderm patterning, with proper regionalization of NE and NPB cells (Fig. 1c and Supplementary Fig. 1). Interestingly, the concentric zone of Pax3+ cells at the colony periphery exhibited a smaller zone width, as characterized by FWHM for spatial distribution of Pax3 intensity (92 μ m), compared with concentric zones of Zic1+ (128 μ m) and Msx1+ (175 μ m) cells, respectively (Supplementary Fig. 1). This observa-

tion is consistent with in vivo findings that ZIC1+ cells also exist in the neurogenic placode region²⁵. Immunostaining and immunoblotting of E-cadherin and N-cadherin at day 2 and day 7 further confirmed successful neural conversion (Supplementary Fig. 2). To confirm differentiation potentials of neuroectoderm tissues after neural induction, they were continuously cultured under a motor neuron differentiation medium²⁶ or a neural crest differentiation medium^{23,24} (Supplementary Fig. 3). Importantly, only putative NE cells at the colony central region differentiated into Olig2+ motor neuron progenitor cells, whereas only putative NPB cells at the

colony periphery differentiated into $Ap2\alpha^+$ and $Sox10^+$ neural crest cells (Supplementary Fig. 3).

We next sought to examine the effect of colony size on selforganized neuroectoderm patterning. To this end, circular adhesive islands with diameters of 300, 400, 500 and 800 µm were fabricated and compared. Neural induction resulted in the emergence of concentric, ring-shaped neuroectoderm tissues with proper regionalization of NE and NPB cells at day 9 for all colonies (Supplementary Fig. 4). Interestingly, the Pax6+ NE circular pattern size and the concentric zone width of Pax3+ NPB cells, as characterized by FWHM for spatial distributions of Pax6 and Pax3 intensities, respectively, appeared relatively constant for colony diameters of 300-500 µm (Supplementary Fig. 4). Notably, neural induction for colonies with a diameter of 800 µm led to marked cell accumulation at the colony periphery on day 9, coinciding with a notable number of Pax3+, Zic1+ and Msx1+ NPB cells at the colony central region (Supplementary Fig. 4). The underlying mechanism leading to this different cell fate distribution remains unclear, and probably involves secondary tissue morphogenesis¹⁸. We further examined neuroectoderm patterning in circular colonies of 400 µm in diameter under two other initial cell seeding density conditions (5,000 cells cm⁻² and 30,000 cells cm⁻²). A seeding density of 5,000 cells cm⁻² led to abnormal neuroectoderm regionalization. Even though a notable number of Pax6+ NE cells appeared at the colony centre, Pax3+, Zic1+ and Msx1+ NPB cells were evident across entire colonies without distinct spatial patterning (Supplementary Fig. 5). Plating cells at 30,000 cells cm⁻² led to the development of multilayered cellular structures by day 9, even though Pax3+ NPB cells still appeared and formed a single peripheral layer enveloping the colony top surface (Supplementary Fig. 5). Together, we identified micropatterned circular colonies of 300-500 µm in diameter and an initial cell seeding density of 20,000 cells cm⁻² as the most suitable conditions for in vitro modelling of neural induction (referred to henceforth as the 'default neural induction' condition). Emergent patterning of neuroectoderm tissues with proper autonomous regionalization of NE and NPB cells was also achieved using another hES cell line (H9) and a human induced pluripotent stem (hiPS) cell line (Supplementary Fig. 6).

We further conducted live-cell assays to examine dynamic neuroectoderm patterning using a Sox10-EGFP bacterial artificial chromosome hES cell reporter line (H9)²³. SOX10 is a specifier gene for neural crest induction at the NPB in vertebrates²⁷. Surprisingly, under the default neural induction condition, GFP+ cells emerged first at the colony periphery on day 6 and continuously increased in number there through day 7 and day 8 (Fig. 1d). This observation was further corroborated by immunofluorescence analysis to examine initial appearances and spatial distributions of Pax6+ NE and Pax3+ NPB cells (Supplementary Fig. 7). Together, the time course of expression of NPB markers Pax3, Zic1 and Msx1 and neural crest marker Sox10 in micropatterned hES cell colonies is consistent with mouse embryo development in vivo²⁷⁻²⁹.

To examine a possible role of cell sorting in neuroectoderm patterning, live-cell imaging was conducted for tracking cell migratory behaviours. Migration of cells, whether located at the colony centre or at peripheral region, was very limited under the default neural induction condition, with an average radial displacement less than 20 µm between days 2 and 4 (Supplementary Fig. 8). Furthermore, cell migration could be well simulated using an unbiased random walk model (Supplementary Fig. 8; see Methods). Thus, cell sorting was unlikely to be responsible for emergent regional neuroectoderm patterning in micropatterned colonies. Together, our data support that autonomous regionalization of NE and NPB cells should probably be attributed to cell-fate-determinant, position-dependent information perceived by differentiating cells that dictates the bifurcation dynamics of NE and NPB lineage commitments.

Gradual cell accumulation at the colony centre (Fig. 1b) suggests cell rearrangement and dynamic morphogenetic processes. Indeed, colonies stained for ZO-1 for visualization of cell-cell junctions revealed that at day 4, cells at the colony periphery displayed a greater projected area than at the colony centre (Supplementary Fig. 9, Supplementary Fig. 10, and Fig. 2a,b). Compared with those at the colony centre, cells at the colony periphery also displayed greater intracellular cytoskeletal contractility, as revealed by stronger staining for phosphorylated myosin and greater traction stress quantitated using PDMS micropost force sensors³⁰ (Fig. 2a,c and Supplementary Fig. 9; see Methods). Supplementing neural induction medium with blebbistatin (10 µM), which inhibits myosin motor activity and thus cytoskeletal contractility, effectively eliminated spatial differences in projected area or traction stress between colony peripheral and central regions at day 4 (Supplementary Fig. 10 and Fig. 2a-c). We note that blebbistatin treatment did not result in notable cell toxicity (Supplementary Fig. 11). However, it decreased cell proliferation and thus effectively increased the cell spreading area at the colony central area (Supplementary Fig. 11). Importantly, even though NE and NBP cells still appeared at day 9 with blebbistatin treatment, proper neuroectoderm regionalization was severely impaired, with abundant Pax3+, Zic1+ and Msx1+ NPB cells randomly distributed across entire colonies (Fig. 2d). Reducing cell seeding density under default neural induction conditions to 5,000 cells cm⁻² also caused more uniform spatial distributions of projected area and traction stress across entire colonies (Supplementary Fig. 10).

Our results in Fig. 2 suggested critical roles of morphogenetic cues in mediating neuroectoderm patterning with proper regionalization. Neural induction in vivo has been shown to be mediated through graded BMP signalling^{8-10,31}. Specifically, a BMP signalling gradient provides positional information in the ectoderm, with high BMP activity promoting epidermal differentiation, low BMP for NP development, and intermediate BMP for NPB specification^{8-10,31} (Fig. 1a). Indeed, we observed strong correlations between spatial regulations of cell shape, cytoskeletal contractility and BMP activity at day 4. Most cells at the colony periphery showed prominent nuclear staining of phosphorylated SMAD 1/5 (p-SMAD 1/5), a downstream target of BMP-SMAD signalling, whereas far fewer cells at the colony central area were p-SMAD 1/5 nuclear positive (Fig. 3a,b). Interestingly, blebbistatin treatment or plating cells at 5,000 cells cm⁻² rescued BMP activity at the colony central area on day 4 (Fig. 3a,b), consistent with their effects on promoting NPB differentiation at the colony central region. Replacing LDN in the default neural induction condition with NOGGIN (100 ng ml⁻¹), a protein that antagonizes BMPs, or dorsomorphin (1 µM), which inhibits BMP receptors, led to similar results of graded SMAD transcriptional activation at day 4 and neuroectoderm regionalization at day 9 (Supplementary Fig. 12).

To specifically examine the functional roles of cell shape and cytoskeletal contractility in BMP activation, microcontact printing was applied to obtain patterned circular single hES cells with prescribed spreading areas (Supplementary Fig. 13 and Fig. 3c). Cytoskeletal contractility of patterned single hES cells correlated positively with spreading area (Supplementary Fig. 13). Importantly, the percentage of patterned single hES cells with dominant nuclear staining of p-SMAD 1/5 also increased with spreading area (Fig. 3c,d). Furthermore, quantitative polymerase chain reaction with reverse transcription (qRT-PCR) analysis revealed greater expression levels of BMP target genes MSX1, ID1 and ID3 in patterned single hES cells with greater spreading areas (Supplementary Fig. 13). Similar observations about BMP target genes were also obtained when seeding hES cells on vitronectin-coated flat PDMS surfaces at different plating densities to effectively modulate spreading area and cytoskeletal contractility (Supplementary Fig. 13).

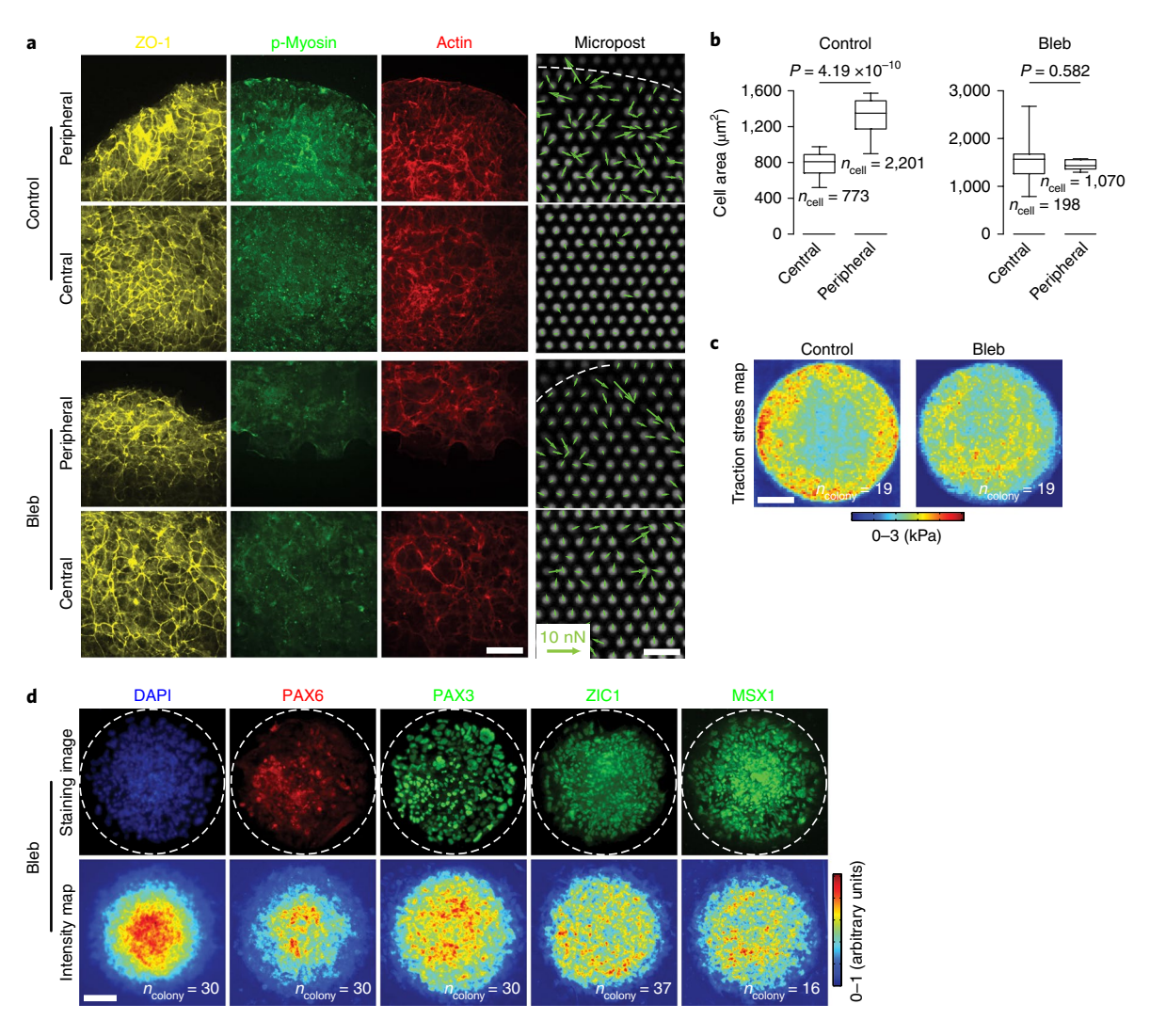


Fig. 2 | **Self-organization of morphogenetic factors controls neuroectoderm patterning. a**, Representative fluorescence images showing staining for ZO-1, phosphorylated myosin (p-myosin) and actin, as well as micropost sensors at colony peripheral and central regions at day 4. hPS cells were cultured in neural induction medium supplemented with either DMSO (control) or blebbistatin (Bleb; $10\,\mu\text{M}$). Circular colonies were divided into two concentric zones ('central' versus 'peripheral') with equal widths. White dashed lines mark the colony periphery. Traction force vectors were superimposed onto individual micropost force sensors. Experiments were repeated three times with similar results. Scale bars, $40\,\mu\text{m}$ (fluorescence micrographs) and $10\,\mu\text{m}$ (micropost images). **b**, Box-and-whisker plots showing projected cell spreading area at day 4 under different conditions as indicated (box, 25-75%; bar-in-box, median; whiskers: 1% and 99%). The number of colonies analysed was pooled from n=3 independent experiments. P values were calculated using unpaired, two-sided Student's t-tests. **c**, Maps showing the spatial distribution of traction stress quantitated using micropost force sensors at day 4 under culture conditions as indicated (see Methods). The number of colonies analysed was pooled from n=3 independent experiments. Data plotted were the mean values. Scale bar, $100\,\mu\text{m}$. **d**, Representative immunofluorescence micrographs and average intensity maps showing colonies at day 9 stained for Pax6, Pax3, Zic1 and Msx1. DAPI counterstained nuclei. White dashed lines mark the colony periphery. Experiments were repeated three times with similar results. The number of colonies analysed was pooled from n=3 independent experiments. Data in intensity maps were the mean values. Scale bar, $100\,\mu\text{m}$.

To further investigate the causal link between cell shape and mechanical force and neuroectoderm patterning, a custom-designed microfluidic cell stretching device was developed and implemented for stretching central regions of micropatterned cell colonies³² (Fig. 4a and Supplementary Fig. 14). Continuous stretching with a square-wave pattern (pulse width of 2 h and period of 4 h) and a 100% stretch amplitude was applied starting from day 2 under the default neural induction condition (Supplementary Fig. 14). Indeed, mechanical stretching enhanced cytoskeletal contractility at the colony central region, as reflected by stronger staining of phosphorylated myosin and actin filaments, compared to unstretched controls (Fig. 4b). Furthermore, stretching of the colony central area effectively rescued nuclear p-SMAD 1/5 and thus BMP activity at the colony central region (Fig. 4c,d). By day 8, a significant number

of Pax3⁺ NPB cells were evident at the colony centre, whereas NE differentiation was completely inhibited there (Fig. 4e). Together, these results unambiguously demonstrate that cell shape and mechanical force can directly activate BMP-SMAD signalling and thus repress NE but promote NPB differentiation.

We next modified the neural induction medium to elucidate the role of BMP signalling in guiding neuroectoderm patterning. Specifically, modulating LDN concentration in neural induction medium resulted in a dose-dependent BMP signalling response. With high-dose LDN (1 μ M), BMP-SMAD signalling was completely repressed across entire colonies at day 4 (Supplementary Fig. 15). Without LDN supplementation, most cells across entire colonies showed prominent nuclear p-SMAD 1/5 at day 4, consistent with BMP activity-inducing properties of the KnockOut Serum

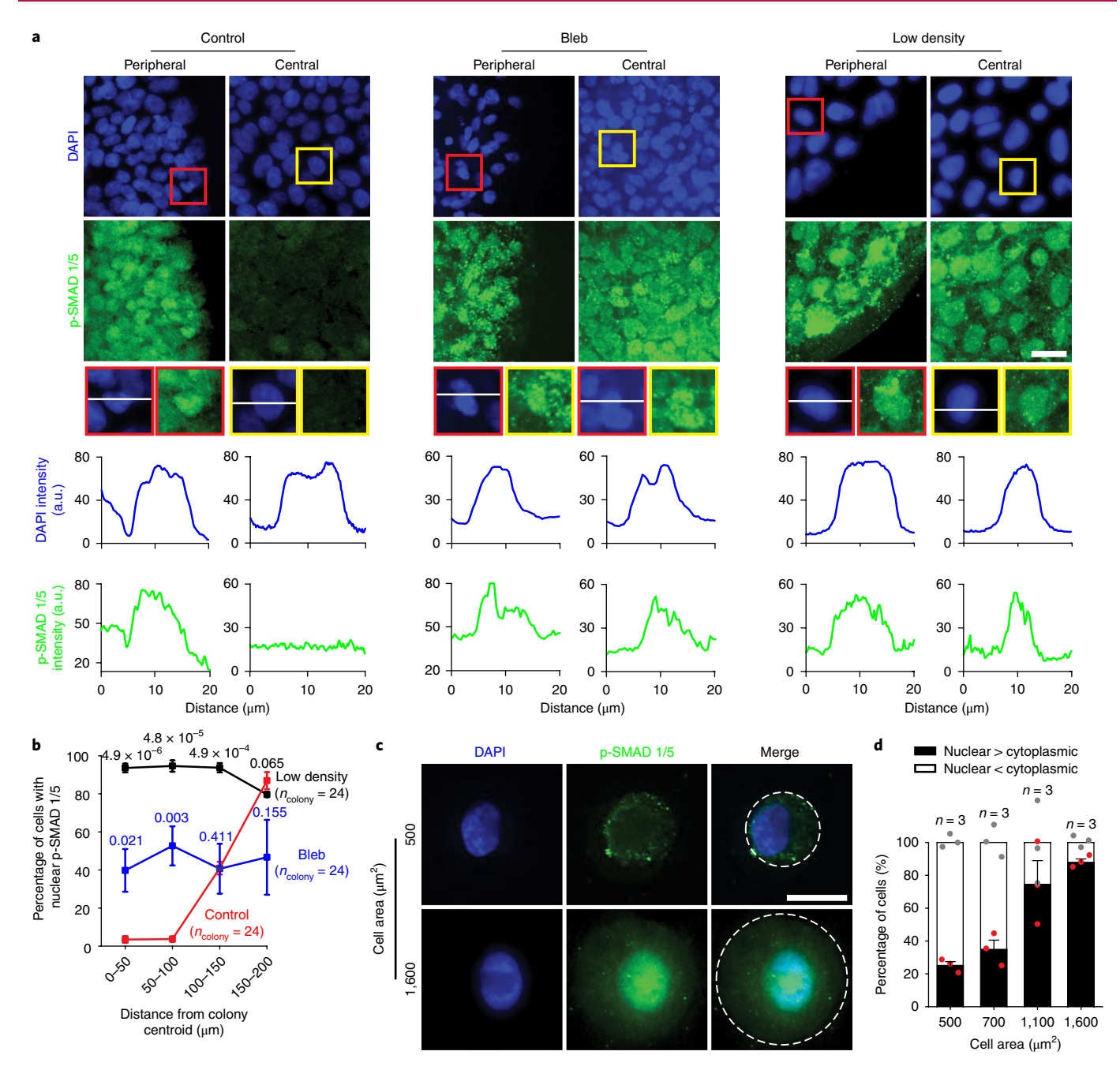


Fig. 3 | Mechanics-guided neuroectoderm patterning is mediated by BMP-SMAD signalling. a, Representative immunofluorescence images showing colony central and peripheral zones at day 4 stained for phosphorylated SMAD 1/5 (p-SMAD 1/5). hPS cells were plated at either 20,000 cells cm⁻² (control) or 5,000 cells cm⁻² (low density) and were cultured in neural induction medium supplemented with either DMSO or blebbistatin (Bleb; $10 \mu M$). Red and yellow rectangles highlight selected peripheral and central regions, respectively, where fluorescence intensities of DAPI and p-SMAD 1/5 were measured along white solid lines drawn across these selected areas. Scale bar, $40 \mu m$. Experiments were repeated three times with similar results. **b**, Percentage of cells with nuclear p-SMAD 1/5 as a function of distance from colony centroid. Based on distance of nuclei from colony centroid, cells were grouped into four concentric zones with equal widths as indicated. The number of colonies analysed was pooled from n = 3 independent experiments. Data were plotted as the mean ± s.e.m. *P* values were calculated between Bleb versus control and low density versus control using unpaired, two-sided Student's *t*-tests. **c**, Representative immunofluorescence micrographs showing patterned circular single hPS cells with defined spreading areas (500 μm² versus 1,600 μm²) stained for p-SMAD 1/5. White dashed lines mark the cell shape. Scale bar, $20 \mu m$. Experiments were repeated three times with similar results. **d**, Bar plot showing percentages of cells with dominant nuclear or cytoplasmic p-SMAD 1/5 as a function of cell spreading area. n = 3 independent experiments. Data were plotted as the mean ± s.e.m.

Replacement (KSR) medium used in the default neural induction condition³³ (Supplementary Fig. 15). Similarly, replacing LDN with BMP4 (25 ng ml⁻¹) in neural induction medium, a condition that promotes BMP signalling, induced prominent nuclear accumulation of p-SMAD 1/5 across entire colonies (Fig. 5a,b). Consequently, by

day 9 at colony centre, NE differentiation was completely inhibited, whereas NPB differentiation was drastically promoted (Fig. 5c). In distinct contrast, replacing KSR serum in the default neural induction condition with the chemically defined Essential 6 medium, a condition that does not promote BMP signalling³⁴, inhibited

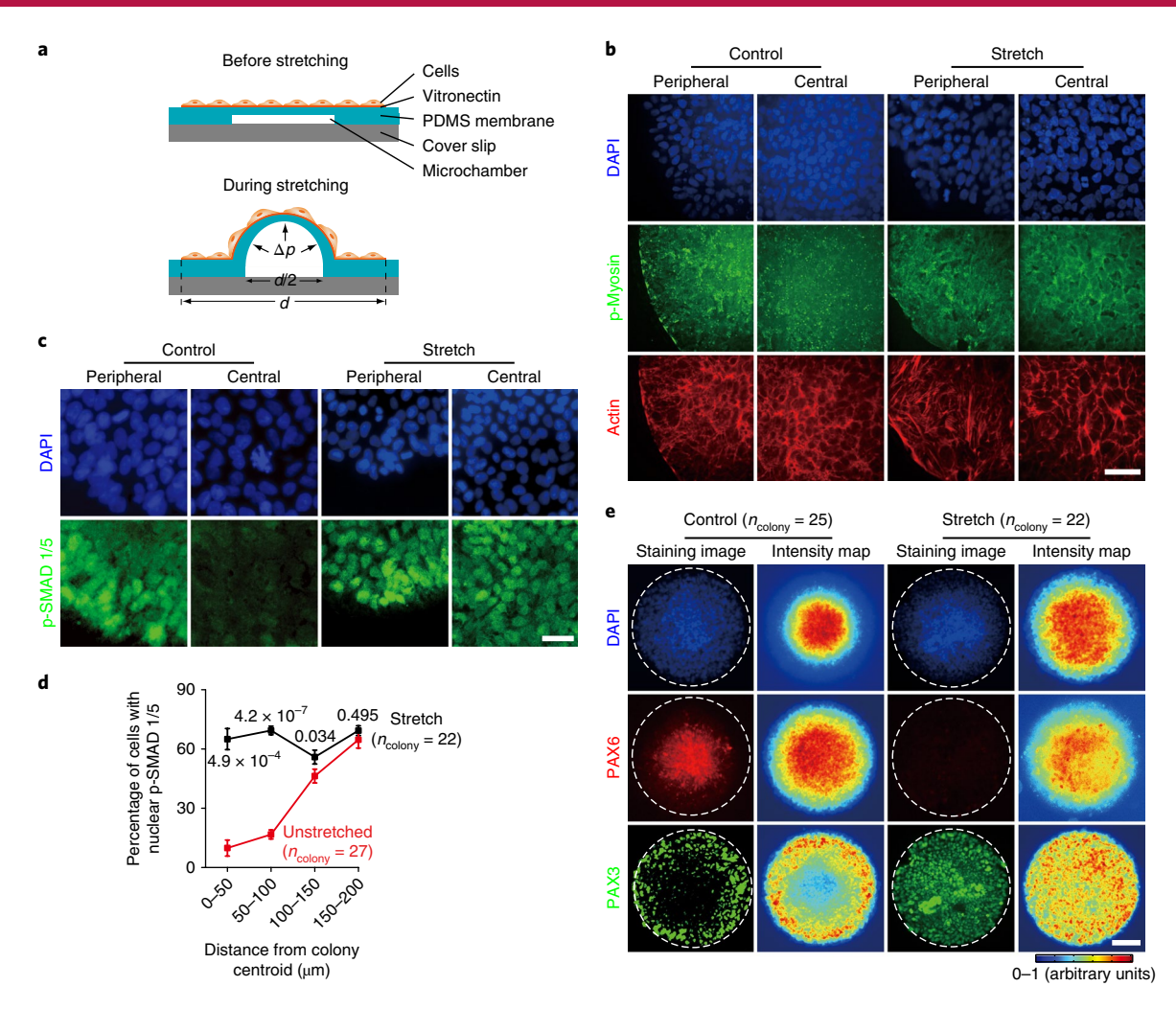


Fig. 4 | Mechanical force is sufficient for activating BMP-SMAD signalling and inducing NPB cell differentiation. a, Schematic of a microfluidic device to apply stretching forces to central zones of micropatterned hPS cell colonies. **b**, Representative fluorescence micrographs showing central and peripheral zones of unstretched (control) and stretched (stretch) micropatterned colonies at day 4 stained for p-myosin and actin. DAPI counterstained nuclei. Scale bar, 40 μm. Experiments were repeated three times with similar results. **c**, Representative immunofluorescence images showing central and peripheral zones of unstretched (control) and stretched (stretch) micropatterned colonies at day 4 stained for phosphorylated SMAD 1/5 (p-SMAD 1/5). DAPI counterstained nuclei. Scale bar, 40 μm. Experiments were repeated four times with similar results. **d**, Percentage of cells with nuclear p-SMAD 1/5 as a function of distance from colony centroid under stretch and unstretched control conditions as indicated. Based on distance of nuclei from colony centroid, cells were grouped into four concentric zones with equal widths as indicated. The number of colonies analysed was pooled from *n* = 4 independent experiments. Data were plotted as the mean ± s.e.m. *P* values were calculated between stretch and unstretched control conditions using unpaired, two-sided Student's *t*-tests. **e**, Representative immunofluorescence micrographs and average intensity maps showing unstretched (control) and stretched (stretch) colonies at day 8 stained for Pax6 and Pax3. DAPI counterstained nuclei. White dashed lines mark the colony periphery. Experiments were repeated three times with similar results. The number of colonies analysed was pooled from *n* = 3 independent experiments. Data in intensity maps were plotted as the mean. Scale bar, 100 μm.

nuclear localization of p-SMAD 1/5 at day 4 and promoted NE differentiation at day 9 across entire colonies (Fig. 5a–c). Consistently, NPB differentiation across entire colonies by day 9 was completely suppressed (Fig. 5c).

Gene expression analysis further confirmed the effect of replacing KSR with Essential 6 on repressing *BMP4* expression (Supplementary Fig. 16). However, replacing LDN with BMP4 in the default neural induction medium upregulated both *BMP4* and *NOGGIN* expression (but not *BMP2*, *BMP6* or *BMP7*), consistent with previous reports^{21,35} (Supplementary Fig. 16). Interestingly, silencing of *BMP4* or *NOGGIN* expression using siRNA did not affect neuroectoderm regionalization in micropatterned colonies (Supplementary Fig. 17), excluding endogenous BMP4 or NOGGIN for instructing NE/NPB patterning.

We further seeded hES cells on flat PDMS surfaces uniformly coated with vitronectin at a low (5,000 cells cm⁻²) or high (50,000 cells cm⁻²) density condition. Consistent with our previous data, the high density condition significantly down-regulated expression of NPB markers *PAX3* and *SOX9* compared with the low density condition (Supplementary Fig. 18). However, exogenously activating BMP by supplementing BMP4 (25 ng ml⁻¹) effectively rescued both *PAX3* and *SOX9* expression (Supplementary Fig. 18). Altogether, our data suggest that morphogenetic cues during emergent neuroectoderm patterning may function upstream of BMP-SMAD signalling to regulate its transcriptional activation (Fig. 5d). Exogenous BMP activation can rescue inhibitory effects of confined cell shape (or small cell spreading area) and impaired cytoskeletal contractile force on BMP signalling.

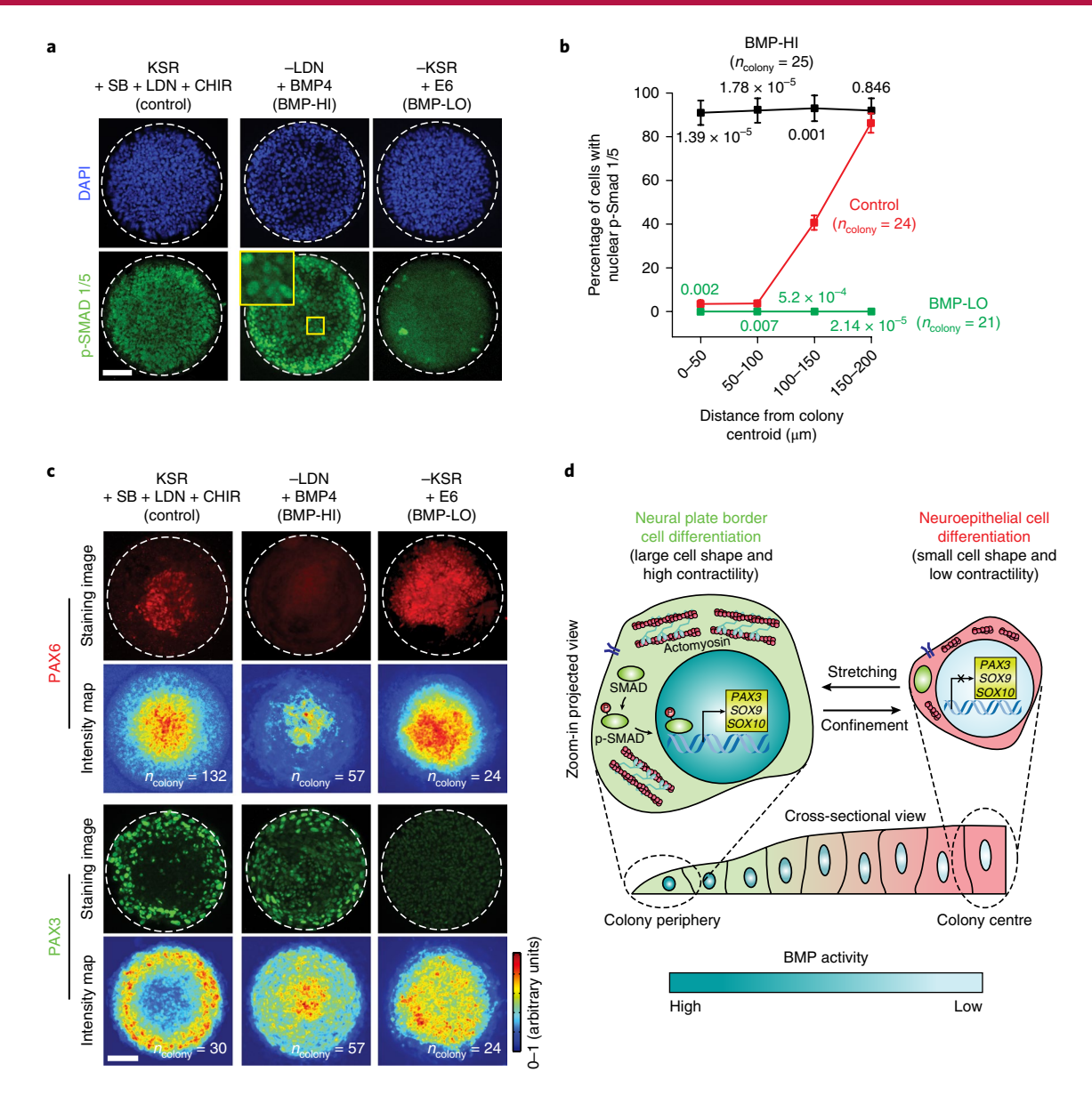


Fig. 5 | BMP-SMAD signalling is required for mechanics-guided neuroectoderm patterning. a, Representative immunofluorescence images showing colonies at day 4 stained for phosphorylated SMAD 1/5 (p-SMAD 1/5). The default neural induction condition (control) was modified as following: – LDN/+BMP4, LDN was replaced with BMP4 (BMP-HI); –KSR/+E6: KSR was replaced with E6 (BMP-LO). CHIR was kept in culture protocols for both BMP-HI and BMP-LO conditions. The zoomed-in image shows a magnified view of the colony central area. Scale bar, 100 μm. Experiments were repeated three times with similar results. **b**, Percentage of cells with nuclear p-SMAD 1/5 as a function of distance from the colony centroid. The number of colonies analysed was pooled from *n* = 3 independent experiments. Data represent the mean ± s.e.m. *P* values were calculated between BMP-HI versus control and BMP-LO versus control using unpaired, two-sided Student's *t*-tests. **c**, Representative fluorescence micrographs and average intensity maps showing colonies at day 9 stained for Pax6 and Pax3. Scale bar, 100 μm. Experiments were repeated three times with similar results. The number of colonies analysed was pooled from *n* = 3 independent experiments. Data in intensity maps represent the mean values. **d**, Geometrical confinement leads to self-organization of morphogenetic factors. Increased cell shape and contractile force at colony periphery result in nuclear accumulation and transcriptional activation of p-SMAD 1/5, which in turn up-regulates NPB specifier genes including *PAX3*, *SOX9* and *SOX10*. Confined cell shape with limited contractile force at the colony centre leads to nuclear exclusion of p-SMAD 1/5 and neuroepithelial differentiation. Modulating cell shape by mechanical stretching or geometrical confinement can thus mediate BMP signalling to regulate neuroectoderm patterning.

Our data, together with others 17,18,20,21,35 , highlight the dependence of fate patterning in hPS cell colonies on both colony geometry and cell density. Etoc et al. recently report a cell density-dependent mechanism for graded BMP signalling involving subcellular lateralization of BMP receptors and diffusion of endogenous NOGGIN 35 . To explore whether this mechanism might be involved in our model, tight-junction integrity was disrupted during neural induction by a brief calcium depletion followed by incubation with Y-27632 (20 μ M), a ROCK (Rho-associated protein kinase) inhibitor, a condition known

to prevent tight junction formation 35,36 (Supplementary Fig. 19). Such treatment has been shown to allow intercellular diffusion of apically delivered TGF- β ligands to bind basolateral receptors and thus restore downstream SMAD activity in high-density epithelial monolayers 35,36 . However, under this tight-junction disruption condition, proper neuroectoderm patterning was still achieved at day 9 (Supplementary Fig. 19), supporting that subcellular lateralization of BMP receptors was unlikely to be responsible for establishing graded BMP signalling in our model.

Recent studies suggest that cell-density-dependent TGF- β inhibition in epithelial cells is due to crosstalk with the Hippo pathway³⁷. The Hippo effector YAP/TAZ is also mechanosensitive and can be regulated by both cell shape and mechanical forces^{38,39}. To examine the role of YAP/TAZ, a small molecular inhibitor cerivastatin (CER), which promotes YAP phosphorylation and thus nuclear exclusion⁴⁰, was supplemented in the default neural induction medium with LDN replaced with BMP4 (25 ng ml⁻¹) to promote BMP activity (Supplementary Fig. 20). Even though nuclear YAP was suppressed across entire colonies at day 4, nuclear localization of p-SMAD 1/5 remained evident and all cells across entire colonies differentiated into Pax3+ NPB cells at day 9. Thus, YAP nuclear translocation did not correlate with p-SMAD 1/5 response, and YAP was unlikely to directly regulate BMP-SMAD signalling and thus neuroectoderm patterning. It remains a future goal to determine how geometrical confinement leads to spontaneous self-organization of morphogenetic factors, how cell shape and cytoskeletal contractility activate BMP-SMAD signalling⁴¹, and how BMP and WNT signals converge to regulate NPB specification^{42,43}.

Our micropatterned neuroectoderm developmental model does not contain non-neural ectoderm or mesenchymal tissues, which may have important roles in instructing neuroectoderm formation in vivo^{8–10}. Nonetheless, there are well documented tissue isolation studies using in vivo models that support neural induction as an autonomous process⁴⁴. The origin of NPB cells is also believed to arise from neural but not epidermal ectoderm^{27,29}. Altogether, our neuroectoderm developmental model is useful for studying self-organizing principles involved in autonomous patterning and regionalization of neuroectoderm tissues.

In this work, we demonstrate that autonomous patterning of neuroectoderm tissue with proper NP and NPB regionalization emerges de novo as the tissue physically takes shape and self-assembles in pre-patterned geometrical confinements. Self-organization of morphogenetic cues, including cell shape and cytoskeletal contractility, can directly feed back to mediate BMP activity and thus dictate spatial regulation of neuroectoderm patterning. Colony geometry can directly influence cell signalling and cell-cell communication through regulatory mechanisms involving dynamic morphogenetic cues and diffusible signals^{17,18,20,21,35}. Such signalling crosstalk involving both biophysical and biochemical determinants may be important in controlling patterning networks to ensure the remarkable robustness and precision of tissue self-organization in vivo¹⁻⁵. We envision that our neuroectoderm developmental model will facilitate future efforts in generating theoretical frameworks that integrate knowledge at the mechanical, cellular and gene-regulatory levels^{17,18,20,21,35}. Future mechanistic investigations of tissue mechanics-guided neuroectoderm patterning will therefore help advance the fundamental understanding of neural development and disease.

Methods

Methods, including statements of data availability and any associated accession codes and references, are available at https://doi.org/10.1038/s41563-018-0082-9.

Received: 8 May 2017; Accepted: 16 April 2018; Published online: 21 May 2018

References

- Wozniak, M. A. & Chen, C. S. Mechanotransduction in development: a growing role for contractility. Nat. Rev. Mol. Cell Biol. 10, 34–43 (2009).
- Keller, R. Physical biology returns to morphogenesis. Science 338, 201–203 (2012).
- 3. Heller, E. & Fuchs, E. Tissue patterning and cellular mechanics. *J. Cell Biol.* **211**, 219–231 (2015).
- Chan, C. J., Heisenberg, C.-P. & Hiiragi, T. Coordination of morphogenesis and cell-fate specification in development. Curr. Biol. 27, R1024–R1035 (2017).

- Gilmour, D., Rembold, M. & Leptin, M. From morphogen to morphogenesis and back. *Nature* 541, 311–320 (2017).
- Schroeder, T. E. Neurulation in Xenopus laevis. An analysis and model based upon light and electron microscopy. J. Embryol. Exp. Morphol. 23, 427–462 (1970).
- Colas, J.-F. & Schoenwolf, G. C. Towards a cellular and molecular understanding of neurulation. *Dev. Dynam.* 221, 117–145 (2001).
- Munoz-Sanjuan, I. & Brivanlou, A. H. Neural induction, the default model and embryonic stem cells. Nat. Rev. Neurosci. 3, 271–280 (2002).
- Stern, C. D. Neural induction: old problem, new findings, yet more questions. Development 132, 2007–2021 (2005).
- Bier, E. & De Robertis, E. M. BMP gradients: a paradigm for morphogenmediated developmental patterning. Science 348, aaa5838 (2015).
- Vijayraghavan, D. S. & Davidson, L. A. Mechanics of neurulation: From classical to current perspectives on the physical mechanics that shape, fold, and form the neural tube. *Birth Defects Res.* 109, 153–168 (2017).
- 12. Tesar, P. J. et al. New cell lines from mouse epiblast share defining features with human embryonic stem cells. *Nature* **448**, 196–199 (2007).
- O'Leary, T. et al. Tracking the progression of the human inner cell mass during embryonic stem cell derivation. Nat. Biotechnol. 30, 278–282 (2012).
- Nakano, T. et al. Self-formation of optic cups and storable stratified neural retina from human ESCs. Cell Stem Cell 10, 771–785 (2012).
- Lancaster, M. A. et al. Cerebral organoids model human brain development and microcephaly. *Nature* 501, 373–379 (2013).
- Poh, Y.-C. et al. Generation of organized germ layers from a single mouse embryonic stem cell. Nat. Commun. 5, 4000 (2014).
- Warmflash, A. et al. A method to recapitulate early embryonic spatial patterning in human embryonic stem cells. Nat. Methods 11, 847–854 (2014).
- Ma, Z. et al. Self-organizing human cardiac microchambers mediated by geometric confinement. Nat. Commun. 6, 7413 (2015).
- Shao, Y. et al. Self-organized amniogenesis by human pluripotent stem cells in a biomimetic implantation-like niche. *Nat. Mater.* 16, 419–425 (2017).
- Shao, Y. et al. A pluripotent stem cell-based model for post-implantation human amniotic sac development. Nat. Commun. 8, 208 (2017).
- Tewary, M. et al. A stepwise model of reaction-diffusion and positionalinformation governs self-organized human peri-gastrulation-like patterning. *Development* 144. 4298–4312 (2017).
- Chambers, S. M. et al. Highly efficient neural conversion of human ES and iPS cells by dual inhibition of Smad signaling. *Nat. Biotechnol.* 27, 275–280 (2009).
- Mica, Y. et al. Modeling neural crest induction, melanocyte specification, and disease-related pigmentation defects in hESCs and patient-specific iPSCs. Cell Rep. 3, 1140–1152 (2013).
- Tchieu, J. et al. A modular platform for differentiation of human PSCs into all major ectodermal lineages. Cell Stem Cell 21, 399–410 (2017).
- Hong, C. S. & Saint-Jeannet, J. P. The activity of Pax3 and Zic1 regulates three distinct cell fates at the neural plate border. *Mol. Biol. Cell* 18, 2192–2202 (2007).
- Sun, Y. et al. Hippo/YAP-mediated rigidity-dependent motor neuron differentiation of human pluripotent stem cells. *Nat. Mater.* 13, 599–604 (2014).
- Sauka-Spengler, T. & Bronner-Fraser, M. A gene regulatory network orchestrates neural crest formation. *Nat. Rev. Mol. Cell Biol.* 9, 557–568 (2008).
- Walther, C. & Gruss, P. PAX-6, a murine paired box gene, is expressed in the developing CNS. Development 113, 1435–1449 (1991).
- Milet, C. & Monsoro-Burq, A. H. Neural crest induction at the neural plate border in vertebrates. *Dev. Biol.* 366, 22–33 (2012).
- Fu, J. et al. Mechanical regulation of cell function with geometrically modulated elastomeric substrates. *Nat. Methods* 7, 733–736 (2010).
- Wilson, P. A. et al. Concentration-dependent patterning of the Xenopus ectoderm by BMP4 and its signal transducer Smad1. *Development* 124, 3177–3184 (1997)
- 32. Michielin, F. et al. Microfluidic-assisted cyclic mechanical stimulation affects cellular membrane integrity in a human muscular dystrophy in vitro model. *RSC Adv.* 5, 98429–98439 (2015).
- Xu, R.-H. et al. Basic FGF and suppression of BMP signaling sustain undifferentiated proliferation of human ES cells. *Nat. Methods* 2, 185–190 (2005).
- Lippmann, E. S., Estevez-Silva, M. C. & Ashton, R. S. Defined human pluripotent stem cell culture enables highly efficient neuroepithelium derivation without small molecule inhibitors. *Stem Cells* 32, 1032–1042 (2014).
- 35. Etoc, F. et al. A balance between secreted inhibitors and edge sensing controls gastruloid self-organization. *Dev. Cell* **39**, 302–315 (2016).
- Nallet-Staub, F. et al. Cell density sensing alters TGF-β signaling in a cell-type-specific manner, independent from Hippo pathway activation. Dev. Cell 32, 640–651 (2015).

- 37. Varelas, X. et al. The Crumbs complex couples cell density sensing to Hippo-dependent control of the TGF-β-SMAD pathway. *Dev. Cell* **19**, 831–844 (2010).
- Dupont, S. et al. Role of YAP/TAZ in mechanotransduction. Nature 474, 179–183 (2011).
- Wada, K.-I. et al. Hippo pathway regulation by cell morphology and stress fibers. *Development* 138, 3907–3914 (2011).
- 40. Sorrentino, G. et al. Metabolic control of YAP and TAZ by the mevalonate pathway. *Nat. Cell Biol.* **16**, 357–366 (2014).
- 41. Kopf, J. et al. BMP growth factor signaling in a biomechanical context. *BioFactors* **40**, 171–187 (2014).
- de Croz., N., Maczkowiak, F. & Monsoro-Burq, A. H. Reiterative AP2a activity controls sequential steps in the neural crest gene regulatory network. *Proc. Natl Acad. USA* 108, 155–160 (2011).
- 43. Steventon, B. et al. Differential requirements of BMP and Wnt signalling during gastrulation and neurulation define two steps in neural crest induction. *Development* 136, 771–779 (2009).
- 44. Moury, J. D. & Schoenwolf, G. C. Cooperative model of epithelial shaping and bending during avian neurulation: autonomous movements of the neural plate, autonomous movements of the epidermis, and interactions in the neural plate/epidermis transition zone. *Dev. Dynam.* **204**, 323–337 (1995).

Acknowledgements

We thank A. Liu for comments on the manuscript. This work is supported in part by the National Science Foundation (CMMI 1129611 and CBET 1149401 to J.F. and CMMI 1662835 to Y. Sun), the American Heart Association (12SDG12180025 to J.F.)

and the Department of Mechanical Engineering at the University of Michigan. The Lurie Nanofabrication Facility at the University of Michigan, a member of the National Nanotechnology Infrastructure Network funded by the National Science Foundation, is acknowledged for support in microfabrication.

Author contributions

Y. Sun, X.X. and J.F. designed experiments; X.X. and Y. Sun performed differentiation assays; A.R.-I. and Y. Sun developed MATLAB scripts for image processing; X.X., Y. Sun, K.M.A.Y., Y.Z., S.W. and Y. Shao generated and analysed gene expression data; X.X. and Y.Y. conducted cell migration assays; L.S. provided Sox10-EGFP cells; Y. Sun, X.X., Y.C. and J.F. analysed data and wrote the manuscript. J.F. supervised the entire project. All authors edited and approved the manuscript.

Competing interests

The authors declare no competing interests.

Additional information

Supplementary information is available for this paper at https://doi.org/10.1038/ \pm 41563-018-0082-9.

Reprints and permissions information is available at www.nature.com/reprints.

Correspondence and requests for materials should be addressed to Y.S. or J.F.

Publisher's note: Springer Nature remains neutral with regard to jurisdictional claims in published maps and institutional affiliations.

Methods

Culture medium. PluriQ Human Cell Conditioned Medium (MTI-GlobalStem) was used to support feeder-free growth of hPS cells⁴⁵. The growth medium comprised DMEM/F12 (GIBCO), 20% KnockOut Serum Replacement (KSR; GIBCO), β-mercaptoethanol (0.1 mM; GIBCO), glutamax (2 mM; GIBCO), 1% non-essential amino acids (GIBCO), and human recombinant basic fibroblast growth factor (bFGF, 4 ng ml-1; GlobalStem) as described previously26. The neural induction medium comprised growth medium, TGF-β inhibitor SB 431542 (10 μM; Cayman Chemical) and BMP4 inhibitor LDN 193189 (500 nM; Selleckchem)²². At day 3, CHIR99021 (3 μ M; Cayman Chemical) was added to the neural induction medium and was withdrawn at day 423,24. The motor neuron differentiation medium comprised N2B27 medium, retinoic acid (RA, 1 µM; Stemcell Technologies) and smoothened agonist (SAG, 500 nM; Stemcell Technologies)²⁶. N2B27 medium comprised 1:1 mixture of DMEM/F12 and neurobasal medium (GIBCO), 1% N2 supplement (GIBCO), 2% B-27 supplement (GIBCO), 2 mM glutamax and 1% non-essential amino acids. The neural crest cell differentiation medium comprised N2B27 medium and 3 µM CHIR99021^{23,24}. Culture medium was pre-equilibrated at 37°C and 5% CO₂ before use.

Cell culture. Both H1 hES cell line (WA01, WiCell; NIH registration number: 0043) and Sox10-EGFP bacterial artificial chromosome hES cell reporter line (H9; WA09, WiCell; NIH registration number: 0062) were cultured on mitotically inactive mouse embryonic fibroblasts (MEFs; GlobalStem) in growth medium. Another H9 hES cell line was cultured using mTeSR1 medium (Stemcell Technologies) and lactate dehydrogenase-elevating virus (LDEV)-free hES cell-qualified reduced growth factor basement membrane matrix Geltrex (Thermo Fisher Scientific) as described previously¹⁹. The hiPS cell line, a gift from P. H. Krebsbach, was cultured in PluriQ Human Cell Conditioned Medium on tissue culture dishes coated with poly[2-(methacryloyloxy)ethyl dimethyl-(3-sulfopropyl) ammonium hydroxide]¹⁶.

The STEMPRO EZPassage Disposable Stem Cell Passaging Tool (Invitrogen) was used for passaging the H1 and Sox10-EGFP hES cell lines every 5 d as described previously 26 . A modified pasteur pipette was used to remove differentiated cells under a stereomicroscope (Olympus). After brief treatment with TrypLE Select (Invitrogen) to release MEFs, the remaining cells were collected using a cell scraper (BD Biosciences) before being transferred onto a tissue culture dish coated with gelatin (Sigma) and incubated for 45 min. Contaminating MEFs would attach to the dish. hES cells in suspension were then collected, centrifuged and re-dispersed in growth medium supplemented with Y27632 (10 μ M; Enzo Life Sciences) before cell seeding. For H9 hES and hiPS cells, cells were digested using TrypLE Select before cell seeding 19 .

The Human Pluripotent Stem Cell Research Oversight Committee at the University of Michigan have approved all protocols for the use of hPS cells. All cell lines were authenticated by Cell Line Genetics as karyotypically normal and were tested negative for mycoplasma contamination using the LookOut Mycoplasma PCR Detection Kit (Sigma-Aldrich).

Microcontact printing. Soft lithography was used to generate patterned PDMS stamps from silicon moulds fabricated using photolithography and deep reactiveion etching (DRIE), as described previously 30. These PDMS stamps were used to generate micropatterned cell colonies and patterned single cells using microcontact printing. Briefly, to generate patterned cell colonies and single cells on flat PDMS surfaces, round glass coverslips with a diameter of 18 mm (Fisher Scientific) were spin-coated (Spin Coater; Laurell Technologies) with a thin layer of PDMS prepolymer comprising the PDMS base monomer and curing agent (10:1 w/w; Sylgard 184, Dow-Corning). PDMS was then thermally cured at 110 °C for at least 24 h. In parallel, PDMS stamps were immersed in a vitronectin solution (20 μg ml⁻¹; Trevigen) for 1 h before being blown dry under nitrogen. Vitronectin has been reported to support self-renewal of hPS cells46. Vitronectin-coated PDMS stamps were then placed in conformal contact with ultraviolet ozone-treated PDMS on coverslips (ozone cleaner; Jelight). After removing PDMS stamps, coverslips were sterilized using ethanol (Fisher Scientific). Protein adsorption to PDMS surfaces not coated with vitronectin was prevented by immersing coverslips in 0.2% Pluronics F127 NF solution (BASF) for 30 min. Coverslips were rinsed with PBS before placed into tissue culture plates for cell seeding. For micropatterned cell colonies, PDMS stamps containing circular patterns with diameters of 300, 400, 500 and 800 µm were used. For patterned single cells, PDMS stamps containing circular patterns with diameters of 25, 30, 37 and 45 µm were used.

To apply continuous stretching to the central zone of micropatterned cell colonies, microcontact printing was performed to print circular adhesive patterns with a diameter of 400 μm onto the deformable PDMS membrane on top of pressurization compartments (with a diameter of 200 μm) in a custom-designed microfluidic cell stretching device. To this end, a custom desktop aligner designed for fabrication of multilayer microfluidic devices was used⁴⁷. Briefly, the vitronectin-coated PDMS stamp and the microfluidic cell stretching device were mounted onto the top and bottom layer holders of the aligner, respectively. Under a digital microscope, the $X/Y/\theta$ stage holding the bottom layer holder was carefully adjusted to align the PDMS stamp and the microfluidic cell stretching device. The PDMS stamp was then gently pressed to achieve conformal contact with the

microfluidic cell stretching device to transfer vitronectin from the stamp to the PDMS membrane on top of the pressurization compartments.

Stencil micropatterning. The stencil was generated by punching through-holes into a PDMS membrane using a 500 μ m biopsy puncher (Fisher Scientific). To generate the PDMS membrane, PDMS prepolymer was spun on a silicon wafer before PDMS was thermally cured a 60 °C for at least 24 h. The PDMS membrane was then peeled off the silicon wafer before punching through-holes into the membrane. Coverslips were immersed in a vitronectin solution (20 μ g ml $^{-1}$) for 1 h before the PDMS stencil was placed onto the coverslip for cell seeding.

Immunocytochemistry. As described previously²⁶, 4% paraformaldehyde (Electron Microscopy Sciences) was used for cell fixation before permeabilization with 0.1% Triton X-100 (Roche Applied Science). Primary antibodies listed in Supplementary Table 2 were then used for protein detection. For immunolabelling, goat-anti mouse AlexaFluor 488 and/or goat-anti rabbit AlexaFluor 546 secondary antibodies were used. To label actin microfilaments, AlexaFluor 555 conjugated phalloidin (Invitrogen) was used. Cells were stained with 4,6-diamidino-2-phenylindole (DAPI; Invitrogen) to visualize the nucleus.

Image analysis. Fluorescence images were recorded using either an inverted epifluorescence microscope (Zeiss Axio Observer Z1; Carl Zeiss MicroImaging) equipped with a monochrome charge-coupled device (CCD) camera or an Olympus DSUIX81 spinning disc confocal microscope equipped with an EMCCD camera (iXon X3, Andor). Fluorescence images of micropatterned cell colonies were first cropped using a custom-developed MATLAB program (MathWorks; https://www.mathworks.com/) to a uniform circular size (as defined by colony size) with pattern centroids aligned. Owing to intrinsic inhomogeneous cell seeding, multilayered cellular structures would inevitably appear in micropatterned cell colonies. These multilayered colonies were excluded from data analyses. Fluorescence intensity of each pixel in cropped images was normalized by the maximum intensity identified in each image. These normalized images were stacked together to obtain average intensity maps. To normalize fluorescence intensities of cell lineage markers by DAPI intensity, the intensity of cell lineage markers for each pixel was divided by the corresponding DAPI intensity. These DAPI-normalized images were stacked together to obtain average DAPInormalized intensity maps. To plot average intensity as a function of distance from colony centroid, average intensity maps for circular cell colonies were divided into 100 concentric zones with equal widths. The average pixel intensity in each concentric zone was calculated and plotted against the mean distance of the concentric zone from colony centroid. From average intensity plots of cell lineage markers, values of the FWHM were determined as the difference between the two radial positions at which the average fluorescence intensity of individual markers is equal to half of its maximum value. The FWHM for average DAPI intensity plots was determined by first calculating the half width at half maximum (HWHM), which was determined as the radial position at which the average DAPI intensity is equal to half of its maximum value at the colony centroid. the FWHM for average DAPI intensity plots was then calculated as double the HWHM.

Colony thickness and nucleus orientation were determined manually with ImageJ (https://imagej.nih.gov/) using confocal images showing X-Z sections of cell colonies stained for N-cadherin. Normalized nucleus dimension was further calculated as the ratio of the height to the width of a circumscribed rectangle bounding the nucleus. Projected cell areas were quantified with the CellProfiler program in ImageJ using immunofluorescence images showing ZO-1 staining. Briefly, nuclei stained by DAPI were used for identification of each cell as primary objects in CellProfiler. ZO-1 staining images were first filtered to remove background before being segregated using a propagation method to determine cell area. To determine projected cell area for central and peripheral zones of cell colonies, a binary circular mask with a diameter of half of the actual pattern diameter was used to crop the original cell colony images. Cells falling on the mask boundary were excluded from quantification. Immunofluorescence images showing p-SMAD 1/5 staining were analysed manually using ImageJ. Cells with nuclear p-SMAD 1/5 were identified as those showing dominant nuclear fluorescence and absence of cytoplasmic fluorescence. Conversely, cells with cytoplasmic p-SMAD 1/5 were identified as those showing absence of nuclear fluorescence. To quantify the spatial distribution of BMP-SMAD activation, circular colonies were divided into four concentric zones with equal widths. The percentage of cells with nuclear p-SMAD 1/5 in each zone was then calculated and plotted against the distance from colony centroid.

Tracking cell migration and unbiased random walk model. On day 0 before cell seeding, hPS cells were labelled with CellTracker Red CMTPX Dye (ThermoFisher Scientific) for 30 min. Labelled hPS cells were mixed with unlabelled cells at a ratio of 1:7 before the cell mixture was seeded onto coverslips containing micropatterned circular adhesive islands. From day 2 ($t=0\,\mathrm{h}$) to day 4, live cell imaging was conducted using the Zeiss Axio Observer Z1 inverted epifluorescence microscope enclosed in the XL S1 incubator (Carl Zeiss MicroImaging) to maintain cell culture at 37 °C and 5% CO₂. Both bright field and fluorescence images were recorded every 20 min for a total of 41 h. All time-lapse images were reconstructed

using Image-Pro Plus (http://www.mediacy.com/imageproplus) to generate TIFF stacks for cell migration tracking. For each image, peripheries of each individual CellTracker labelled cells were marked manually. Positions of cell centroids were then identified from each image to calculate end-to-end cell displacement D and radial displacement during cell migration as a function of time. For radial displacement calculations, cells were divided into two groups based on their radial positions relative to the colony centroid at t=0 h (R_0) ('central' $0 \le R_0 \le 100$ µm; 'peripheral' $100 < R_0 \le 200$ µm). If labelled hPS cells divided during cell migration tracking, one of the daughter cells was randomly selected to continue tracking.

An unbiased random walk model was used for modelling cell migration during emergent neuroectoderm patterning in micropatterned circular hPS cell colonies. In this model, cells move randomly without any preferred migration direction. Cell centroids at each time step n (denoted here as \mathbf{D}_n) can be calculated as $\mathbf{D}_n = \mathbf{D}_{n-1} + AV \gamma$, where A is a random variable following a uniform distribution on [0,1] and γ is a random unit direction vector. Parameter V denotes the maximum cell centroid displacement during each time step, and it can be obtained through least-squares fitting of the experimental data of mean square end-to-end cell displacement D^2 using the expression $D^2 = V^2 t/4$.

Cell viability and proliferation assays. Cell viability was determined using the Live/Dead, Viability/Cytotoxicity Kit (ThermoFisher Scientific) according to the manufacturer's instructions. On day 4 and day 8, culture medium was replaced with fresh medium containing ethidium homodimer (EthD-1; $4\,\mu M$). After incubation for 30 min, fluorescence images were recorded using the Zeiss Axio Observer Z1 inverted epifluorescence microscope to quantify the number of dead cells in each colony.

The Click-iT EdU Alexa Fluor 488 Imaging Kit (ThermoFisher Scientific) was used to measure cell proliferation according to the manufacturers' instructions. Briefly, on day 3, half of the culture medium was replaced with fresh medium containing EdU (20µM). Cells were incubated for 2h before being fixed, permeabilized and incubated with the Click-iT reaction cocktail for 30 min. Cell nuclei were counterstained with DAPI. Cells were then examined under fluorescence microscopy (Zeiss Axio Observer Z1) to detect EdU-stained cell nuclei.

Traction force measurement. Traction force was analysed using PDMS micropost arrays (PMAs) as described previously 30 . Briefly, PMAs were first prepared for cell attachment using microcontact printing to coat micropost top surfaces with vitronectin. To quantify the traction forces of micropatterned cell colonies or single cells, microcontact printing was used to define circular adhesive patterns of different sizes. PMAs were labelled with Δ^9 -DiI (5 µg ml $^{-1}$; Invitrogen) for 1 h. Protein adsorption to all PDMS surfaces not coated with vitronectin was prevented by incubating in 0.2% Pluronics F127 NF solution (BASF) for 30 min.

Live cell imaging was conducted using the Zeiss Axio Observer Z1 inverted epifluorescence microscope enclosed in the XL S1 incubator. Images of micropost tops were recorded using a 40× (for single cells) or 20× (for colonies) objective (Carl Zeiss MicroImaging). All images were recorded at day 4 and were analysed using a custom-developed MATLAB program (MathWorks), as described previously¹⁸, to obtain traction force maps. To determine average traction stress maps for micropatterned cell colonies, individual traction force maps were first adjusted to the same size before being stacked together to obtain average traction stress maps. To plot average traction stress as a function of distance from the colony centroid, circular colonies were first divided into 20 concentric zones with equal widths. The average traction stress in each concentric zone was then calculated and plotted against the mean distance of the concentric zone from the colony centroid.

Microfluidic cell stretching device. The microfluidic cell stretching device comprised a PDMS structural layer, a PDMS inlet block and a glass coverslip. The PDMS structural layer, which contained a microfluidic network for applying pressures to simultaneously activate 64 pressurization compartments to induce PDMS membrane deformation, was fabricated using soft lithography. Briefly, the PDMS prepolymer was spin-coated onto a silicon mould generated using photolithography and DRIE. The PDMS layer was thermally cured at 110 °C for at least 24 h before being peeled off the silicon mould. An inlet for fluid connections was then punched into the PDMS structural layer using a 1 mm biopsy punch (Fisher Scientific). Both the coverslip and the PDMS structural layer were briefly cleaned with 100% ethanol (Fisher Scientific) and blown dry under nitrogen before

being treated with air plasma (Plasma Prep II; SPI Supplies) and bonding together. In parallel, another PDMS block was prepared, and an inlet for fluid connection was punched into the PDMS block with a 0.5 mm biopsy punch. After treating both with air plasma, the PDMS block and the PDMS structural layer were bonded together with their fluid inlets aligned manually. The microfluidic cell stretching device was baked at 110 °C for at least another 24h to ensure robust bonding between different layers. Deionized water was injected into the microfluidic cell stretching device before applying pressure through a microfluidic pressure pump (AF1, Elveflow). Elveflow Smart Interface software (https://www.elveflow.com/) was used for programming the pressure pump for continuous cell stretching with a square-wave pattern (pulse width of 2 h, period of 4 h and 50% duty cycle).

RNA isolation and qRT-PCR analysis. As described previously 36 , RNA was extracted from cells using the RNeasy kit (Qiagen) following the manufacturer's instructions. A CFX Connect SYBR Green PCR Master Mix system (Bio-Rad) was used for qRT-PCR. For relative quantification, human TBP primer was used as an endogenous control. An arbitrary Ct value of 40 was assigned to samples in which no expression was detected. Relative expression levels were determined by calculating $2^{-\Delta\Delta Ct}$ with the corresponding s.e.m. All analyses were performed with at least three biological replicates and three technical replicates.

Western blotting. As described previously²⁶, whole cell lysates were prepared and separated on SDS-polyacrylamide gel before being transferred to PVDF membranes. PVDF membranes were then incubated with blocking buffer (Li-Cor) for 1h before being soaked with primary antibodies overnight at 4°C. Blots were then incubated with IRDye secondary antibodies (Li-Cor) for 1h. An Odyssey Sa Infrared Imaging System (Li-Cor) was used for protein expression detection. Uncropped scans of Western blots are shown in Supplementary Fig. 2.

siRNA knockdown. As described previously²⁶, hPS cells were transfected with *BMP4* or *NOGGIN* siRNA and scramble control using Viromer Blue (OriGene). Briefly, cells were plated at 80% confluence on vitronectin-coated 6-well plates and subjected to siRNA transfection the next day. After 24h, transfected cells were seeded onto coverslips containing micropatterned circular adhesive islands. Three additional siRNA treatments were conducted at days 2, 4 and 6 after cell seeding.

Pharmacological treatment. To inhibit actomyosin contractility, blebbistatin ($10\,\mu$ M in DMSO; Cayman Chemical) was added to culture medium from day 1 till cell fixation. To modulate BMP signalling, recombinant human BMP4 ($25\,\mathrm{ng}\,\mathrm{ml}^{-1}$; R&D Systems) was added to the neural induction medium.

Statistics. Statistical analysis was performed using Excel (Microsoft; https://www.microsoft.com). The statistical significance between two groups was analysed by a two-sided Student's *t*-test. In all cases, a *P* value of less than 0.05 was considered statistically significant.

Reporting Summary. Further information on experimental design is available in the Nature Research Reporting Summary linked to this article.

Code availability. MATLAB scripts used in this work are available from the corresponding authors upon reasonable request.

Data availability. Data supporting the findings of this study are available within the article and its Supplementary Information files and from the corresponding authors upon reasonable request.

References

- Villa-Diaz, L. G. et al. Synthetic polymer coatings for long-term growth of human embryonic stem cells. Nat. Biotechnol. 28, 581–583 (2010).
- Braam, S. R. et al. Recombinant vitronectin is a functionally defined substrate that supports human embryonic stem cell self-renewal via αVβ5 integrin. Stem Cells 26, 2257–2265 (2008).
- 47. Li, X. et al. Desktop aligner for fabrication of multilayer microfluidic devices. *Rev. Sci. Instrum.* **86**, 075008 (2015).
- Weng, S. et al. Mechanosensitive subcellular rheostasis drives emergent single-cell mechanical homeostasis. *Nat. Mater.* 15, 961–967 (2016).



Corresponding author(s): Jianping Fu and Yubing Sun

Life Sciences Reporting Summary

Nature Research wishes to improve the reproducibility of the work that we publish. This form is intended for publication with all accepted life science papers and provides structure for consistency and transparency in reporting. Every life science submission will use this form; some list items might not apply to an individual manuscript, but all fields must be completed for clarity.

For further information on the points included in this form, see Reporting Life Sciences Research. For further information on Nature Research policies, including our data availability policy, see Authors & Referees and the Editorial Policy Checklist.

Please do not complete any field with "not applicable" or n/a. Refer to the help text for what text to use if an item is not relevant to your study. For final submission: please carefully check your responses for accuracy; you will not be able to make changes later.

Experimental design

1. Sample size

Describe how sample size was determined.

All experiments were conducted with at least two independent experiments and multiple biological replicates. Sample sizes were determined based on our previous experience and similar studies of other groups. Sample sizes were determined as sufficient since they led to similar results.

2. Data exclusions

Describe any data exclusions.

Due to intrinsic inhomogeneous cell seeding, some multilayered cellular structures would inevitably appear in micropatterned cell colonies. These multilayered colonies were excluded from data analyses. When quantifying cell morphological features and nuclear staining as a function of different regions of micropatterned cell colonies, those cells falling on region boundaries were excluded from quantification. This information is explained in the "Image analysis" section of the Methods.

3. Replication

Describe the measures taken to verify the reproducibility of the experimental findings.

Reported results were repeated and confirmed for at least two independent experiments. Key experimental findings were reliably reproduced by two investigators involved in this work

4. Randomization

Describe how samples/organisms/participants were allocated into experimental groups.

Samples were randomly allocated to control and different experimental groups (see Methods). However, no particular randomization method was used in this work.

5. Blinding

Describe whether the investigators were blinded to group allocation during data collection and/or analysis.

Investigators were not blinded to group allocation, as no animal/human studies were conducted in this manuscript.

Note: all in vivo studies must report how sample size was determined and whether blinding and randomization were used.

6.	Statistical	parameters

For all figures and tables that use statistical methods, confirm that the following items are present in relevant figure legends (or in the Methods section if additional space is needed).

n/a	Confirmed
	The exact sample size (n) for each experimental group/condition, given as a discrete number and unit of measurement (animals, litters, cultures, etc.)
	A description of how samples were collected, noting whether measurements were taken from distinct samples or whether the same sample was measured repeatedly
	A statement indicating how many times each experiment was replicated
	The statistical test(s) used and whether they are one- or two-sided Only common tests should be described solely by name; describe more complex techniques in the Methods section.
	A description of any assumptions or corrections, such as an adjustment for multiple comparisons
	Test values indicating whether an effect is present Provide confidence intervals or give results of significance tests (e.g. P values) as exact values whenever appropriate and with effect sizes noted.
	A clear description of statistics including <u>central tendency</u> (e.g. median, mean) and <u>variation</u> (e.g. standard deviation, interquartile range)
	Clearly defined error bars in <u>all</u> relevant figure captions (with explicit mention of central tendency and variation)

See the web collection on statistics for biologists for further resources and guidance.

▶ Software

Policy information about availability of computer code

7. Software

Describe the software used to analyze the data in this study.

MATLAB, ImageJ, Image-Pro Plus were used for image analysis. Elveflow Smart Interface was used for programming pressure pump. Excel (Microsoft) was used for statistics.

For manuscripts utilizing custom algorithms or software that are central to the paper but not yet described in the published literature, software must be made available to editors and reviewers upon request. We strongly encourage code deposition in a community repository (e.g. GitHub). *Nature Methods* guidance for providing algorithms and software for publication provides further information on this topic.

Materials and reagents

Policy information about availability of materials

8. Materials availability

Indicate whether there are restrictions on availability of unique materials or if these materials are only available for distribution by a third party.

All materials used in this work are commercially available. There is no restriction on availability of any materials used in this work.

9. Antibodies

Describe the antibodies used and how they were validated for use in the system under study (i.e. assay and species).

Only certified and company-validated antibodies were used in this work for Western blotting (WB) or immunocytochemistry (ICC):

ZO-1, Invitrogen (33-9100), 1:50 (ICC)

PAX6, Abcam (ab78545), 1:200 (ICC)

PAX3, Novus (NBP1-32944), 1:200 (ICC)

ZIC1, Novus (NB600-488), 1:200 (ICC)

MSX1, Novus (NBP2-30052), 1:200 (ICC)

p-SMAD 1/5, Millipore (AB3848), 1:500 (WB) and 1:100 (ICC)

p-MLC, Cell Signaling (3671S), 1:50 (ICC)

GAPDH, Santa-Cruz Biotechnology (sc-25778), 1:200 (WB)

N-CADHERIN, Abcam (ab12221), 1:100 (ICC) and 1:500 (WB)

E-CADHERIN, BD Biosciences (610181), 1:100 (ICC) and 1:500 (WB)

OLIG2, Santa-Cruz Biotechnology (sc-48817), 1:100 (ICC)

NESTIN, Santa-Cruz Biotechnology (sc-23927), 1:100 (ICC)

MAP2, Sigma-Aldrich (M1406-.2ML), 1:100 (ICC)

SOX10, Cell Signaling (89356S), 1:100 (ICC)

AP2α, Santa-Cruz Biotechnology (sc-12726), 1:100 (ICC)

The antibody information (including species, application, and catalog number) has been provided in Supplementary Information (Supplementary Table 2). All antibodies have been validated by the companies from which they were purchased from. The subcellular localization of all the proteins analyzed in this work has been previously reported. This information was used to further validate the specificity of antibodies.

10. Eukaryotic cell lines

a. State the source of each eukaryotic cell line used.

The following cell lines were used in this work: H1 hES cell line (WA01, WiCell; NIH registration number: 0043)

H9 hES cell line (WA09, WiCell; NIH registration number: 0062) A hiPS cell line that is reported in Villa-Diaz, L. G. et al. Nat. Biotechnol. 28, 581 (2010)

b. Describe the method of cell line authentication used.

All hPS cell lines have been authenticated by the original sources and also authenticated inhouse by immunostaining for pluripotency markers and successful differentiation to the three germ layer cells.

c. Report whether the cell lines were tested for mycoplasma contamination.

All cell lines used in this work have been tested negative for mycoplasma contamination.

d. If any of the cell lines used are listed in the database of commonly misidentified cell lines maintained by ICLAC, provide a scientific rationale for their use.

No commonly misidentified cell lines listed by ICLAC were used in this work.

▶ Animals and human research participants

Policy information about studies involving animals; when reporting animal research, follow the ARRIVE guidelines

11. Description of research animals

Provide all relevant details on animals and/or animal-derived materials used in the study.

Irrelevant to this work. This work doesn't involve animal or animal-derived materials.

Policy information about studies involving human research participants

12. Description of human research participants

Describe the covariate-relevant population characteristics of the human research participants. Irrelevant to this work. This work doesn't involve human or human samples.